Continuous Fixed Bed CO2 Adsorption: Breakthrough, Column Efficiency, Mass Transfer Zone

Authors:

Mohammed K. Al Mesfer, Mohd Danish, Mohammed Ilyas Khan, Ismat Hassan Ali, Mudassir Hasan, Atef El Jery

Abstract:

The increased levels of carbon dioxide in the environment have incited the search for breakthrough technologies to lessen its impact on climate. The CO2 capture from a mixture of CO2/N2 was studied using a molecular sieve (MS) and silica gel type-III. The breakthrough behavior was predicted as a function of temperature, superficial velocity, and CO2 partial pressure. The breakpoint time reduced significantly with increased temperature and increased superficial velocity. The CO2 adsorption capacity increased appreciably with decreased temperature and increased CO2 pressure. The saturation CO2 adsorption capacity from the CO2/N2 mixture reduced appreciably with increased temperature. The molecular sieve contributed to higher adsorption capacity, and the highest CO2 uptake of 0.665 mmol/g was realized for MS. The smaller width of the mass transfer zone and higher column efficiency of 87.5% for MS signify the efficient use of the adsorbent; this lowers the regeneration cost. The findings suggest that a molecular sieve is suitable for CO2 capture due to high adsorption performance owing to better adsorption characteristic parameters.

Article

Continuous Fixed Bed CO$_2$ Adsorption: Breakthrough, Column Efficiency, Mass Transfer Zone

Mohammed K. Al Mesfer [1], Mohd Danish [1,*], Mohammed Ilyas Khan [1] , Ismat Hassan Ali [2] , Mudassir Hasan [1] and Atef El Jery [1]

[1]   Chemical Engineering Department, College of Engineering, King Khalid University, Abha 61411,
     Saudi Arabia; almesfer@kku.edu.sa (M.K.A.M.); mkaan@kku.edu.sa (M.I.K.); m-hasan@kku.edu.sa (M.H.);
     ajery@kku.edu.sa (A.E.J.)
[2]   Chemistry Department, College of Science, King Khalid University, Abha 61411, Saudi Arabia;
     ismathassanali@gmail.com
*   Correspondence: mdansh@kku.edu.sa; Tel.:+96-658-054-0101

check for
updates

Abstract: The increased levels of carbon dioxide in the environment have incited the search for breakthrough technologies to lessen its impact on climate. The CO$_2$ capture from a mixture of CO$_2$/N$_2$ was studied using a molecular sieve (MS) and silica gel type-III. The breakthrough behavior was predicted as a function of temperature, superficial velocity, and CO$_2$ partial pressure. The breakpoint time reduced significantly with increased temperature and increased superficial velocity. The CO$_2$ adsorption capacity increased appreciably with decreased temperature and increased CO$_2$ pressure. The saturation CO$_2$ adsorption capacity from the CO$_2$/N$_2$ mixture reduced appreciably with increased temperature. The molecular sieve contributed to higher adsorption capacity, and the highest CO$_2$ uptake of 0.665 mmol/g was realized for MS. The smaller width of the mass transfer zone and higher column efficiency of 87.5% for MS signify the efficient use of the adsorbent; this lowers the regeneration cost. The findings suggest that a molecular sieve is suitable for CO$_2$ capture due to high adsorption performance owing to better adsorption characteristic parameters.

Keywords: bed capacity; breakthrough behavior; greenhouse gases; mass transfer zone; column efficiency

1. Introduction

Greenhouse gases have become a consequential global issue, and CO$_2$ is the most abundant greenhouse gas (GHG), which is significantly contributing to changes in the global climate. An escalating concentration of GHGs in the surroundings is detrimental to health, the natural landscape, the prosperity of every living organism, and our lifestyle. The vital source of CO$_2$ is carbon-releasing fuels such as petroleum, coal, natural gas, and other nonrenewable sources [1]. Fossil-fuel-based power plants can be categorized as possible prime sources of CO$_2$ emission, and the utilization of fossil fuels contributes to three-quarters of the increase in carbon dioxide emissions [2]. The Intergovernmental Panel on Climate Change (IPCC) mentioned that CO$_2$ is a consequential GHG produced as the outcome of human action [3]. The global carbon dioxide concentration has risen by about 100 ppm in the last 250 years [4]. The depletion of CO$_2$ emissions appears to be the foremost task [5,6]. There are three techniques, i.e., post-combustion, pre-combustion, and oxy-fuel methods to capture CO$_2$, depending on the plant layout [1,7–9]. The leading technologies, i.e., physical and chemical absorption [10], membrane separation [11], and cryogenic separation [12], are in practice for CO$_2$ capture. Additionally, the sorption generally refers to absorption, adsorption, both absorption and adsorption, and desorption. Post-combustion capture is characterized by the key benefit of curbing

GHG emissions owing to its compatibility with retrofitted technologies for combustion [13]. The most feasible process for CO_2 captures for power plants on a short time-scale is post-combustion [14–17]. An adsorption for GHG control is an effective process that can be employed to reduce CO_2 emissions into the atmosphere [5,18]. To curb the greenhouse effect, adsorption is considered an effective technology to capture CO_2 from flue gas [19,20]. The industrial adsorbent is regenerated either by increasing the temperature known as temperature swing adsorption (TSA) or by reducing the pressure termed as pressures swing adsorption (PSA). Vacuum swing adsorption (VSA) is a technique also used for the regeneration of the adsorbent bed, in which the process swings to a vacuum to regenerate the adsorbent.

A yellow tuff was utilized as an adsorbent for CO_2 capture in fixed bed columns, and an adsorption capacity of 0.710 mmol/g at 20 °C was reported, emphasizing thermodynamics and the kinetics of the process [21]. A thorough review of various carbon capture methodologies has been carried out, including absorption, cryogenic separation, membrane separation, and adsorption, with a focus on kinetics, process parameters, thermodynamics, and scale-up [22]. A critical review of metal–organic framework (MOF) synthesis and utilization for CO_2 capture has been carried out [23]. Research progress has been extensively reviewed from experimental results to molecular simulations in MOFs for CO_2 adsorption, storage, and separations. Various types of porous media have been synthesized for CO_2/CH_4 separations [24] at 273 and 298 K. The highest adsorption capacity of 8.36 mmol/g was obtained at 273 K for activated carbon. The fixed-bed CO_2 capture from the CO_2/N_2 feed was investigated using porous carbon produced from walnut shells, with a prediction of 1.58 mmol/g separation capacity at 293 K [25]. An activated carbon fiber was prepared, and an adsorption capacity of 1.3 mmol/g was reported [26] at 25 °C and 101.3 kPa. It was also suggested that CO_2 uptake under operating conditions can be correlated with narrow micropore volume. A low-cost carbon black-coated with fine particles of magnetite was developed for CO_2 adsorption–desorption study, and CO_2 uptake of nearly 0.58 mmol/g at 18 °C and 1 atm was attained [27]. The Avrami kinetic model was found to best fit the data, and a deactivation model was used to analyze the dynamic CO_2 adsorption response. Activated carbon was prepared from coals by treatment with KOH, NaOH, and $ZnCl_2$ at different temperatures (600–800 °C), and a capacity of adsorption equal to 9.09 mmol/g was reported for KOH [28].

An experimental analysis focused on breakthrough behavior was conducted by utilizing pitch-based activated carbon beads [29]. The effect of feed rate, composition, operating pressure, and temperature on the adsorption process was investigated. A purity of 93.7% and recovery of 78.23% was obtained with the feeding of 15% CO_2 at 303 K and 202.65 kPa. A parametric study and breakthrough behavior, with specific emphasis on the mass transfer zone by utilizing two grades of activated carbons using fixed-bed columns, have been carried out [30,31]. Activated carbon was used for CO_2 capture by temperature swing adsorption (TSA), and the result showed that CO_2 adsorption/desorption using activated carbon is affected differently by pressure and temperature [32]. The effect of the acoustic field on CO_2 desorption using activated carbon in a fluidized bed was investigated using the TSA technique [33], and considerable enhancement in desorption efficiency was reported. The beads of activated carbon were employed to examine the adsorption equilibrium with a feed mixture of CO_2 and N_2 [34], and a CO_2 adsorption capacity of 1.92 mmol/g was reported at 303 K and 100 kPa. The data were very well fitted by the virial adsorption equation and the multisite Langmuir model. Activated carbon and N-enriched activated carbon were utilized for CO_2 separation, and the breakthrough curve was replicated [35]. The breakthrough curves in the fixed-bed column were obtained at different temperatures and a total pressure of 1.01 bar. The breakthrough curves were reproduced satisfactorily using the linear driving force (LDF) model. The applicability of the PSA technique for CO_2 capture in coal-fired power plants has been gauged [36], and the results obtained were found to be promising. The molecular sieves are porous, synthetic zeolite crystals, metal aluminosilicates. The sieves are separated by adsorption, according to molecular polarity and

degree of unsaturation, and are regenerated by heating or elution. Silica gel is a hard, granular, and very porous product made from gel precipitated by acid treatment of sodium silicate solution.

The zeolites, activated carbon, and molecular sieve type adsorbents were employed to explore the kinetics and equilibrium [37]. The adsorption isotherm was observed to follow typical type-I isotherms, signifying a monolayer adsorption mechanism, and maximal adsorption capacity was obtained for activated carbon. The effect of superficial velocity on the breakthrough behavior utilizing MOF, activated carbons, and crystalline pellets was studied [38]. It was observed that the difference between the stoichiometric time, considering constant and variable velocities, grows exponentially with adsorbate concentration in the feed. A feed concentration of 20% results in a shift of breakthrough time of 6% and a deviation in the equilibrium amount adsorbed of 6% for the gases that adsorb more strongly, such as CO_2 on activated carbon. An adsorption study of CO_2 separation, utilizing activated carbons, zeolites, and carbon nanotubes, has been examined, and the maximum capacity was reported for activated carbons among all the adsorbents [39]. A synthesized hybrid adsorbent with 13X and activated carbon were used as an adsorbent for CO_2 separation, and maximum adsorption capacity of 2.63 mmol/g was exhibited for hybrid adsorbent [40]. A MOF (UTSA-16) was utilized for CO_2 separation and was reported to have the highest adsorption capacity of 160 cm^3/cm^3 [41]. The adsorption of polyaspartamide adsorbent was predicted using both the kinetic/nonkinetic models [42], and it was suggested that the external mass transfer attributed to adsorption of the adsorbate. The effect of flow rates, feed concentrations, and temperature on the breakthrough response for CO_2 adsorption was investigated using immobilized polyethylenimine on mesoporous silica in a fluid bed, with emphasis on the mass transfer zone [43]. The kinetic process is better explained by a pseudo-first-order kinetic model.

A brief summary of the adsorption capacity reported for employing various types of adsorbents is presented in Table 1. A CO_2 capture study [44] using zeolite 13X from a mixture of CO_2/N_2 was performed, and the highest CO_2 uptake of 4.9 mmol/g was reported at 22 °C and 1.5 atm. The investigators [45] applied zeolite 13X for adsorption equilibrium of methane, CO_2, and nitrogen and reported a CO_2 capture capacity of 4.61 mmol/g at 1 atm and 22 °C. Two grades of adsorbents, i.e., molecular sieve (MS) 13X and MS 4A were used, and the highest adsorption capacity of 3.2 mmol/g was attained for MS 13X at 25 °C and 1 atm [46]. The effect of bed temperature on the CO_2 desorption equilibrium of the zeolite bed was studied with an adsorption capacity of 2.18 mmol at 20 °C and 0.15 atm [47]. Zeolites were used for CO_2, N_2, and Ar adsorption, with maximal CO_2 uptake of 6.3 mmol/g for 13X at a low temperature of 5 °C and 0.9 atm [48].

Table 1. Adsorption capacity of various adsorbents.

Adsorbent	Temperature (°C)	Pressure (atm)	Adsorption Capacity (mmol/g)	References
Zeolite 13X	20	0.15	2.63	[44]
Zeolite 13X	22	1.5	4.90	[44]
Zeolite 13X	22	1	4.61	[45]
Molecular sieve 13X	25	1	3.2	[45]
Molecular sieve 13X	20	0.15	2.18	[47]
Molecular sieve 4A	25	1	2.7	[46]
Molecular sieve 4A	20	0.15	1.65	[47]
13X	5	0.9	6.3	[48]
5A	5	0.7	5.46	[48]
ZSM-5	40	0.1	0.32	[49]
ZSM-5	30	1	1.60	[49]

A study [49] focused on adsorption separation of CO_2/CH_4 was carried out at different temperatures of 30 and 40 °C, and a capacity of 1.6 mmol/g was reported at 30 °C and 1 atm. The objective of the current study is to investigate the packed bed adsorption of CO_2 from a CO_2/N_2 mixture using a molecular sieve and silica-gel-type adsorbents. The bed temperature, superficial velocity, and CO_2

equilibrium partial pressure are considered to determine the breakthrough behavior and bed capacity. The bed characteristic parameters, i.e., column efficiency, width of mass transfer zone, and usable bed height at breakpoint are determined. The originality of the work is to analyze the relative contribution of each operating parameter on the adsorption capacity, utilizing both types of adsorbents.

2. Materials and Methods

2.1. Materials

The commercially available adsorbents of different sizes, i.e., molecular sieve (MS; average size: 3.0×10^{-3} m, mass: 240 g) and silica gel type-III (SG; average size: 2.0×10^{-3} m, mass: 300 g), procured from Sigma Aldrich (Steinheim, Germany) were used to conduct the experiments. SG activation was carried out at a temperature of 120 °C for 2 h using a drying oven (ELE International, range: 0–400 °C) to remove any traces of water, whereas MS was activated at a temperature of 200 °C for 2 h to remove any traces of water and volatile compounds. Both types of adsorbents were characterized by a Quantachrome NovaWin-NOVA surface analyzer. The adsorbents were kept in air-tight bottles after drying and before charging the adsorbent to the column. The morphological characteristics of MS and SG were obtained using a JEOL scanning electron microscope (SEM) (JSM-6360 LA, Akishima, Tokyo, Japan). The compositions of the adsorbents were determined using Energy Dispersive X-Ray Spectroscopy (EDS) equipped with SEM. The gases CO_2 and N_2 (purity > 99.999%) were purchased from a local supplier (Abdulla Hashim gas) of Abha of Asser Province, Kingdom of Saudi Arabia.

2.2. Setup

A stainless steel (SS) column (Figure 1), with an effective column length of 0.240 m and an internal diameter of 0.045 m, was utilized for the experimental study. The column was made of steel and jacketed all around to control the bed temperature. The water enters the column jacket at the lower side and leaves from the top side of the column. The hole at the top-side of the column is used for filling and emptying the column with the desired adsorbents. The column bypass is incorporated for calibration purpose and it includes two 3-way directional valves V3 and V4. The needle valve (V5) is used to control the pressure in the column and this pressure is measure by pressure gauge (P1).
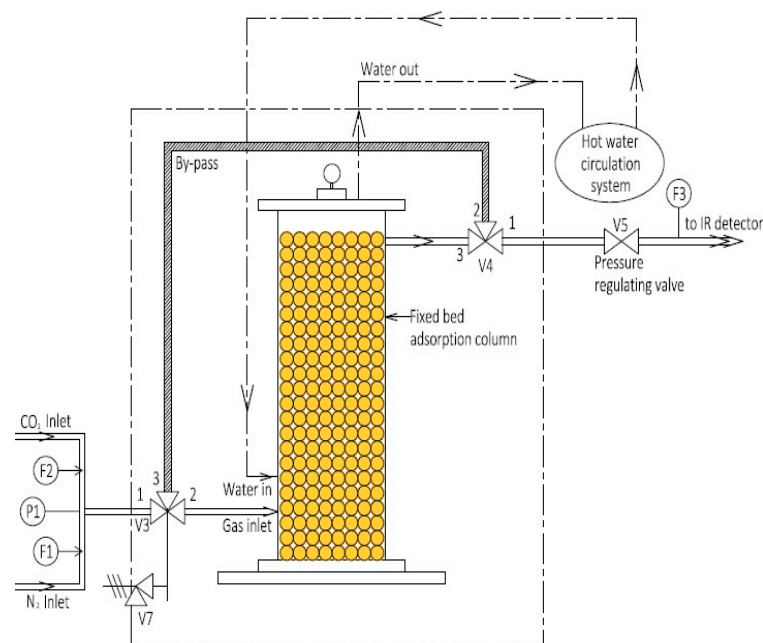
Figure 1. Adsorption unit. V3 and V4: 3-way directional valves; V5: needle valve; P1: pressure gauge; F1 and F2: flow controllers, F1 (N_2), F2 (CO_2).

The mass flow controllers F1 (N_2) and F2 (CO_2) are used to adjust the required flow rates of feed mixture. The six temperature sensors (T1–T6) are located inside the column at definite central positions along the length to record the temperature profiles. The temperatures T1 and T6 represent the top and bottom temperatures of the column, respectively, whereas the temperatures T2–T5 correspond to the intermediate column temperatures from the top to the bottom side. All the temperature sensors are insulated type-K thermocouples. The temperature sensors T1 and T2 are located at 42 and 83 mm away from the top of the column, respectively. The sensors T3 and T4 are positioned at distances of 125 and 167 mm, respectively. Additionally, 208 and 250 mm are the positions of the bottom side temperature sensors T5 and T6, respectively. Temperature sensor T7 measures the temperature of hot water circulator. An infrared (IR) detector measured the exit column CO_2 concentration at a regular time interval of 30 s, recoded using a data logger.

2.3. Procedure

A mixture of N_2 and CO_2 was fed into the bottom of the packed column. Flow meters F1 (for N_2) and F2 (for CO_2) were provided to determine and control the flow rates of gases. The column was filled up to the height of 0.240 m for performing the experiments under the desired set of operating conditions. The flow to the IR sensor was controlled by a flow rate control valve, F3. After the completion of adsorption, the complete bed desorption was carried out by a continuous flow of nitrogen (N_2) for a sufficiently long time before starting the next set of experiments. Complete bed regeneration was ascertained when column exit CO_2 concentration (C_{exit}) was recorded and measured to equal zero (up to two places after decimal points).

3. Results and Discussion

3.1. Adsorbent Characterizations

MS and SG were characterized by a Brunauer–Emmett–Teller (BET) surface analyzer (Quantachrome NoavaWin-NOVA Instruments) for surface area. The surface characteristics of MS and SG are depicted in Table 2. The multipoint surface areas of 362.2 and 556.4 m^2/g were exhibited by MS and SG. The higher value of the Barrett–Joyner–Halenda (BJH) method pore volume of 6.731×10^{-2} cm^3/g for SG was obtained compared to 4.111×10^{-2} cm^3/g for MS. SG exhibited an average pore size of 20.45 Å compared with a higher value of average pore size of 27.52 Å for MS.

Table 2. Adsorbent surface characterization data.

Adsorbent	Surface Area A (m^2/g)	Pore Volume V_p (cm^3/g)	Pore Radius Sp (Å)
Molecular sieve	362.2	4.11×10^{-2}	27.52
Silica gel type-III	556.4	6.731×10^{-2}	20.45

The surface morphological characterizations of MS are presented in Figure 2a,b, and the surface morphological characterizations of SG are shown in Figure 2c,d. It was observed that pore density is significantly higher for MS compared to SG adsorbent and the pores are also uniformly distributed, as depicted in Figure 2a,b. The pores are not consistently distributed, and considerably higher non uniformity in pore size distribution was observed, as shown in Figure 2c,d.
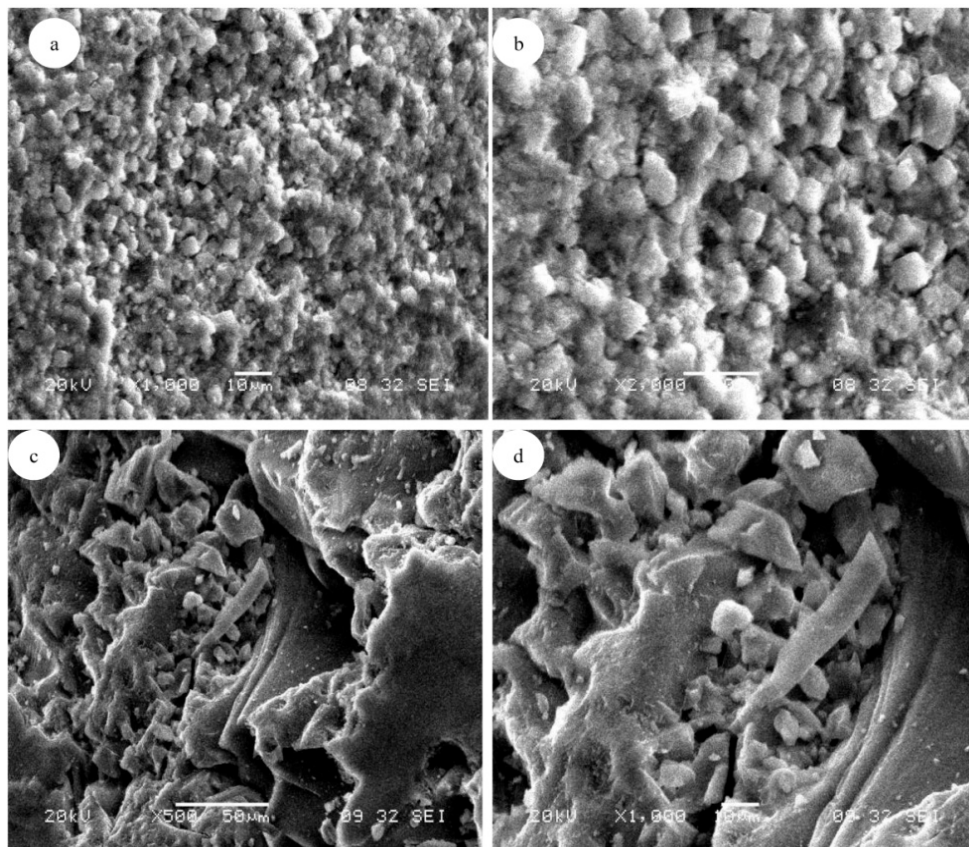
Figure 2. Morphological characteristics: (**a**) scanning electron microscope (SEM) image of molecular sieve (MS) with magnification 1000×; (**b**) SEM image of MS with magnification 2000×; (**c**) SEM images of silica gel (SG) type-III with magnification 500×; (**d**) SEM images of SG type-III with magnification 1000×.

3.2. Molecular Sieve

The adsorption response curves using MS at different column temperatures are depicted in Figure 3a. The adsorption response concentrations (C_{exit}/C_{in}), with adsorption time at bed temperatures of 30, 40, and 50 °C, were analyzed. The data were collected at a superficial velocity of 0.052 m/s, with an initial concentration of CO_2 equal to 5%. The breakthrough time declined with an increase in bed temperature. The time corresponding to C_{exit}/C_{in} = 5% (vol %) is termed the breakthrough time. The delayed breakthrough period was recorded at a bed temperature of 40 °C. Prolonged breakthrough time signifies the better capacity of an adsorbent. The breakthrough time declined from 1230 to 885 s with an increase in bed temperatures from 30 to 50 °C. The adsorption bed reached a condition of breakthrough at a time period of 1110 s with a constant bed temperature of 40 °C. Prolonged breakpoint time at a lower bed temperature is an indication of an enhanced bed capacity of an adsorbent. It was concluded that breakthrough time considerably decreases with an increase in bed temperatures.

In a fixed bed, it is feasible to achieve a nearly solute (CO_2) free gas until the adsorbent in the bed reaches saturation. Consider the flow of fluid containing an adsorbable component through a fixed bed of adsorbent. If external and internal mass transfer resistances are very small, plug flow is achieved, axial dispersion is negligible, the adsorbent is initially free of adsorbent, and adsorption isotherms begins at the origin; then, local equilibrium between the fluid and adsorbent is attained instantaneously, resulting in a shock-like wave called the stoichiometric front, which moves as a sharp concentration front through the bed. After the stoichiometric time, the stoichiometric wave front approaches the end of the column, the CO_2 concentration in the fluid abruptly rises to the initial concentration C_{in}, and, after that, no further adsorption is possible. The extent to which the adsorption capacity of the bed can

be utilized is determined by the steepness of the breakthrough curve (S-shaped). The shape of the S-curve is significant for determining the length of the adsorption column.
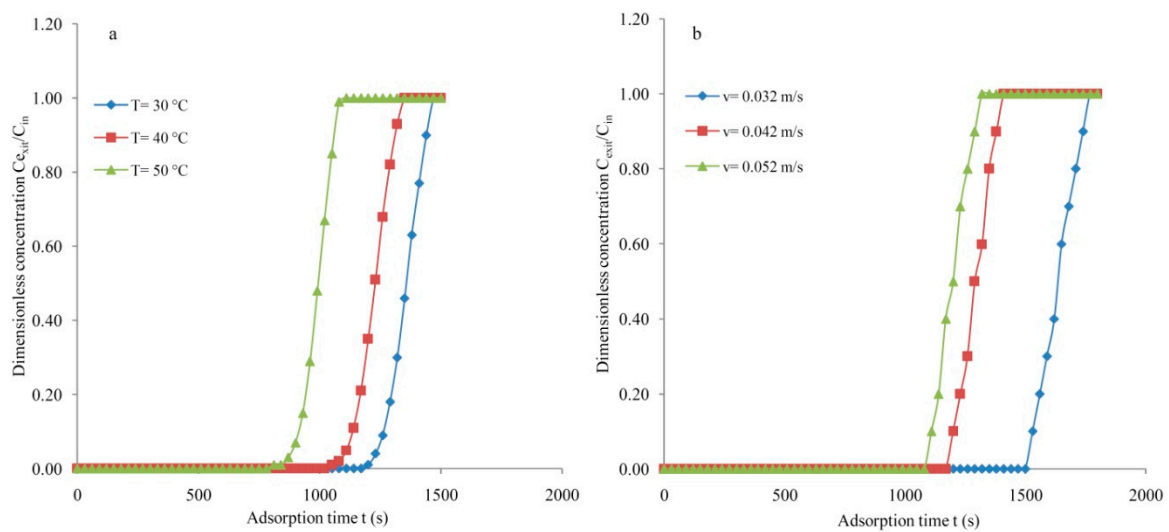
Figure 3. (**a**) Adsorption response curve at different temperatures for MS (v = 0.052 m/s, C_{in} = 5%); (**b**) adsorption response curves at different superficial velocities for MS (T = 40 °C, C_{in} = 5%).

The influence of superficial velocity on the adsorption response employing MS was studied and is depicted in Figure 3b under the constant condition of the bed temperature (40 °C) and the CO_2 inlet concentration in the gaseous feed mixture (5%). The data were collected at three different superficial feed mixture velocities of 0.032, 0.042, and 0.052 m/s. The breakthrough time was reduced with an increase in superficial feed velocity. Lower superficial velocity leads to an increased breakpoint time, resulting in the increased capture capacity of an adsorbent. The breakthrough time of 1515 s was observed at a superficial velocity of 0.032 m/s, and it declined from 1185 s to 1095 s with an increase in the superficial velocity from 0.042 to 0.052 m/s. The longest breakthrough time was attained at a velocity of 0.032 m/s.

The mass-transfer-zone width and shape rely on the adsorption isotherm, flow rate, mass transfer rate to the particles, and diffusion in the pores. The stoichiometric time can be estimated by applying Equation (1):

$$t_{st} = \int_0^{\infty} \left(1 - \frac{C_{exit}}{C_{in}}\right) dt \tag{1}$$

where C_{exit}, C_{in}, and t_{st} are the column outlet, inlet CO_2 concentrations (vol %), and stoichiometric time (s), respectively.

Equation (1) for breakthrough time or any time t, which represents the area above the curve between the limit t = 0 to t = t, can be written as Equation (2):

$$t_{ca} = \int_0^t \left(1 - \frac{C_{exit}}{C_{in}}\right) dt \tag{2}$$

The dynamic adsorption capacity q (mmol/g) of the column corresponding to t_{ca} (or stoichiometric time, t_{st}) is estimated using Equation (3):

$$q = \frac{F\, t_{ca}\, C_{in}}{m} \tag{3}$$

where F is the total feed molar flow rate; C_{in} and m stand for the concentration of CO_2 in the feed stream (vol %) and mass of adsorbent used in the bed, respectively.

The CO_2 adsorption capacity variations with temperature are shown below (Figure 4a). The adsorption data were generated at the bed temperatures of 30, 40, and 50 °C by adjusting the superficial velocity to 0.052 m/s. The maximum adsorption capacity of 0.664 mmol CO_2/g adsorbent was obtained at a bed temperature of 30 °C and reduced to 0.598 mmol/g adsorbent when the column temperature was increased to 40 °C. The adsorption capacity of 0.488 mmol/g adsorbent was obtained at a column temperature of 50 °C. It was found that the maximum capacity of the adsorbent for CO_2 was strongly dependent on the bed temperature and significantly reduces with an increase in bed temperature. The reduced temperature increases the capacity of CO_2 adsorption from the CO_2/N_2 feed mixture. It is also noticed that saturation adsorbent capacity varies significantly with bed temperature. Since adsorption is an exothermic process, the concentration of the adsorbed gas reduces with increasing temperature at a given equilibrium pressure.
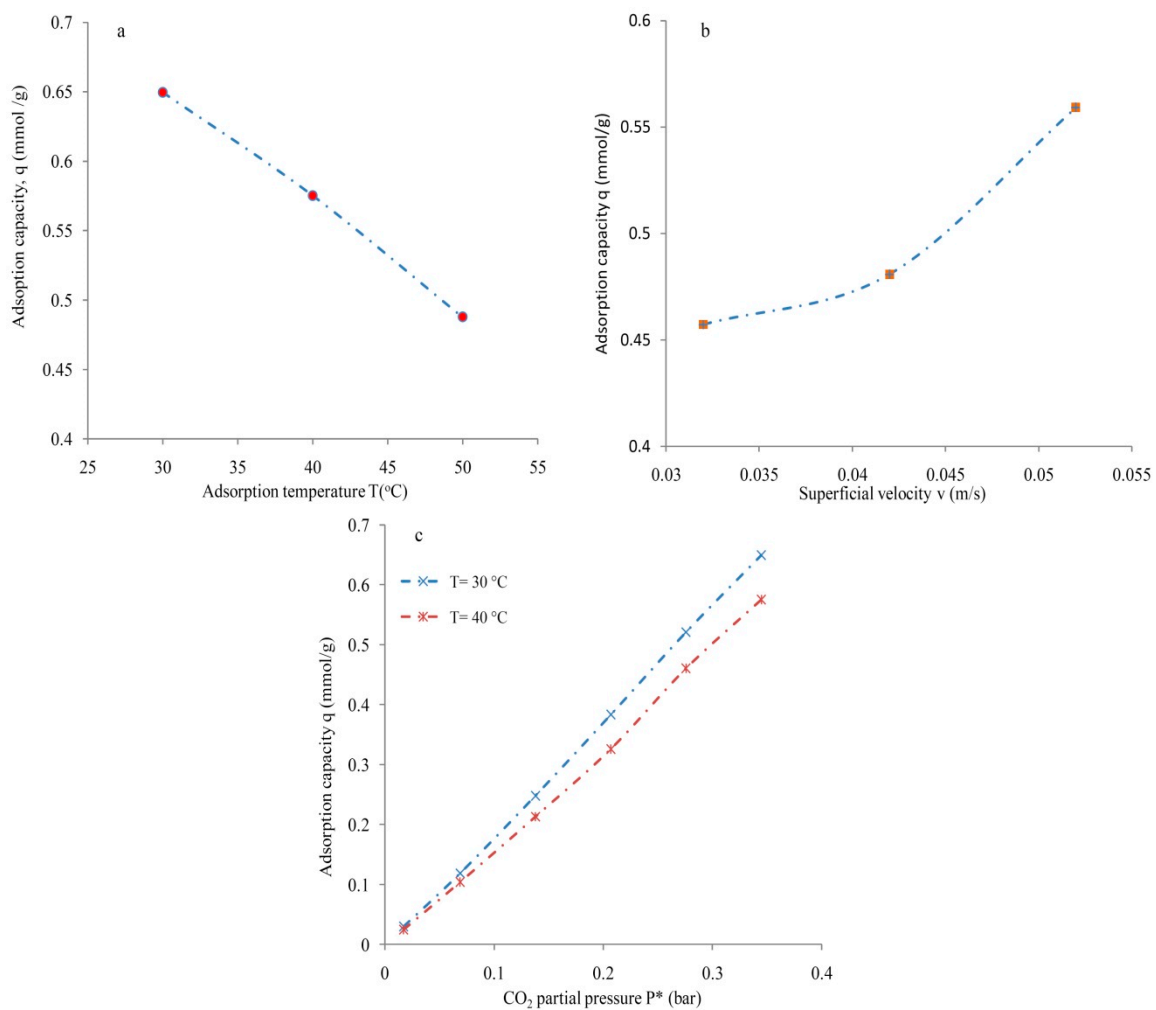

Figure 4. (**a**) Effect of temperatures on the bed capacity for MS (v = 0.052 m/s, C_{in} = 5%); (**b**) effect of the superficial velocity on the adsorption capacity for MS (T = 40 °C, C_{in} = 5%); (**c**) adsorption isotherms for MS (v = 0.052 m/s, C_{in} = 5%).

The relationship between the adsorption capacity and the gaseous feed mixture superficial velocity is depicted in Figure 4b. The experiments were performed at superficial velocities of 0.032, 0.042, and 0.052 m/s. The temperature of the column was adjusted to 40 °C, and the inlet concentration of CO_2 in the feed was fixed at 5% (vol %). It is noticed that the adsorption capacity was enhanced with increased superficial feed velocity. The adsorption capacity of 0.457 mmol CO_2/g adsorbent was estimated at a lower superficial feed velocity of 0.032 m/s. The adsorption capacity increased up to 0.481 mmol/g adsorbent, with an increase in the feed superficial velocity to 0.042 m/s. The maximal capacity of CO_2 separation equal to 0.559 mmol/g adsorbent from the CO_2/N_2 mixture was tabulated at a superficial

velocity of 0.052 m/s. Therefore, it is suggested that high superficial velocity enhances the adsorption capacity of the adsorbent. Thus, it can be concluded that higher superficial velocity increases the adsorption capacity of CO_2 from the CO_2/N_2 gaseous mixture.

The influence of the equilibrium CO_2 partial pressure on CO_2 selective adsorption capacity is depicted in Figure 4c. Adsorption isotherms were reproduced at bed temperatures of 30 and 40 °C. The data were obtained at a superficial velocity of 0.052 m/s when the inlet CO_2 concentration in the feed mixture was fixed at 5% (vol %). It was found that adsorption capacity strongly depends on the equilibrium partial pressure of the CO_2. An adsorption capacity of 0.029 mmol/g was reported as corresponding to a partial pressure of 0.017 bar for an isotherm produced at 30 °C. The maximum adsorption capacity of 0.650 mmol/g adsorbent was obtained at a pressure of 0.345 bar. The capacity of adsorption at the breakthrough point was estimated to be equal to 0.029 mmol/g. The adsorption capacity of 0.025 mmol/g adsorbent was predicted at a partial pressure of 0.017 bar, corresponding to the breakthrough point at 40 °C. It was noticed that adsorption capacity increases almost linearly with equilibrium partial pressure. The saturation bed capacity at 40 °C isotherm was equal to 0.575 mmol/g. The temperature profiles inside the column for MS and SG are shown in Figure 5a,b, respectively. The increase of temperature above the set point (40 °C) for MS is significantly higher than the temperature observed for SG. Owing to the exothermic nature of adsorption, the mass transfer front is followed by a rise of temperature supported by temperature profiles at different positions. It may also be concluded that as the concentration of CO_2 rises, the heat generated due to adsorption leads to an increased temperature inside the fixed-bed column.
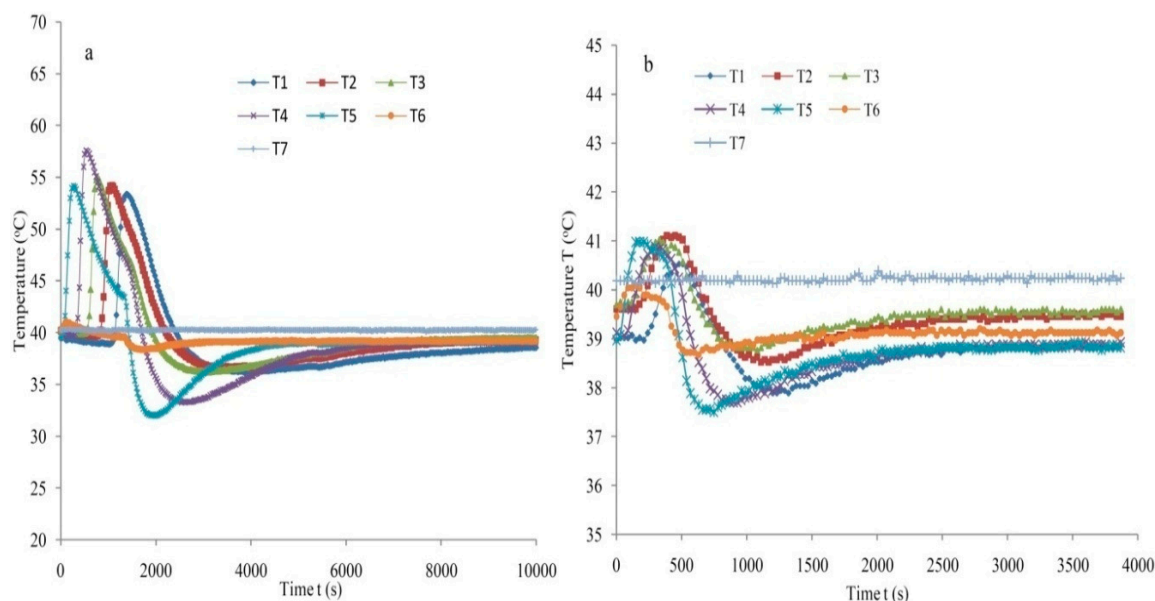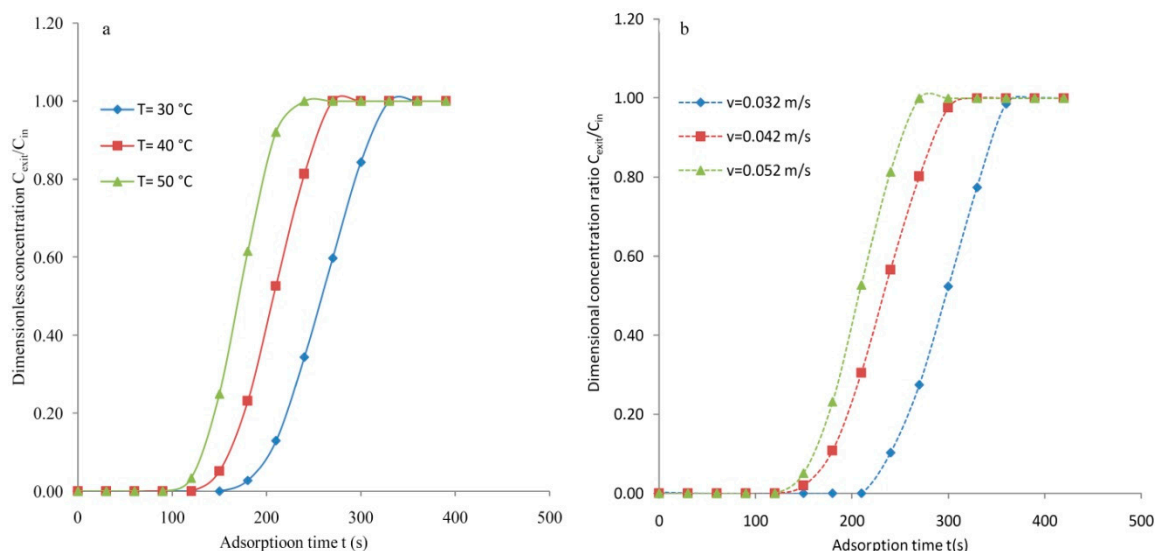

Figure 5. Adsorption–desorption temperature profiles for (**a**) MS; (**b**) SG. T1-T7: temperature sensors.

3.3. Silica Gel Type-III

A breakthrough adsorption study employing SG adsorbent was conducted. The detailed BET characterization was carried out, and their results are presented in Table 2. The adsorption responses at different column temperatures are plotted, as shown in Figure 6a. The data were generated at a superficial velocity of 0.052 m/s with C_{in} = 5%. The column temperatures were adjusted to 30, 40, and 50 °C to analyze the influence of temperature on breakthrough. The breakthrough time declined with an increase in the bed temperature, which signifies the increment of the adsorption capacity with temperature. The maximum breakthrough time of 185 s was recorded at a fixed bed temperature of 30 °C. The breakthrough time of 185 s decreased to 150 s with an increase in temperature from 30 to

40 °C. The S-shape curves (breakthrough curve) obtained for the SG adsorbent are less steep compared with those obtained for MS.


Figure 6. (**a**) Adsorption response curves at different temperatures for SG (v = 0.052 m/s, C_{in} = 5%); (**b**) adsorption response curves at different superficial velocities for SG (T = 40 °C, C_{in} = 5%).

The influence of the superficial velocity on the adsorption response with time is depicted in Figure 6b. The experiments were conducted at a fixed temperature of 40 °C, and inlet CO_2 was adjusted at 5% in the feed mixture. The superficial velocities of 0.032, 0.042, and 0.052 m/s were chosen to analyze the adsorption response. The maximum breakthrough period of 220 s was observed at the superficial velocity of 0.032 m/s. The breakthrough point declined from 220 to 160 s, with an increase in the superficial feed velocity from 0.032 to 0.042 m/s. The breakthrough time of 150 s was achieved at a feed superficial velocity of 0.052 m/s. The minimum breakthrough time of 125 s was achieved at the bed temperature of 50 °C. It may be concluded that the influence of the feed's superficial velocity on breakpoint time is significant and more pronounced at lower superficial velocity. It can be suggested that a longer breakthrough period signifies an enhanced adsorption capacity at reduced column temperatures.

The adsorption responses in terms of adsorption capacity for SG with bed temperature are depicted in Figure 7a. The data were obtained at a superficial velocity of 0.052 m/s by fixing the CO_2 percentage in the feed at 5% (vol %). It was found that the maximum adsorption capacity varied inversely with bed temperature. The maximum adsorption capacity of 0.099 mmol CO_2/g adsorbent was obtained, corresponding to a bed temperature of 30 °C, but declined to 0.077 mmol CO_2/g adsorbent with an increased adsorption temperature to 40 °C. Additionally, at a column temperature of 50 °C, the adsorption capacity of the adsorbent further reduced to 0.064 mmol CO_2/g.

It can be concluded that saturation bed capacity declined significantly with an increase in the bed temperature. The saturation capacity obtained by employing SG is considerably lower compared with that obtained for MS. The adsorption capacities of 0.664 and 0.099 mmol/g were estimated under a constant condition of bed temperature (T = 30 °C), with superficial velocity v = 0.052 m/s, for MS and SG, respectively. The results of the feed superficial velocity on the maximum adsorption capacity employing SG are depicted in Figure 7b. The experiment was performed at an adsorption temperature of 40 °C by controlling the initial concentration at 5%. It was observed that the adsorption capacity of the adsorbent enhanced notably with an increase in the feed superficial velocity from 0.032 to 0.052 m/s. The adsorption capacity of 0.069 mmol/g was estimated to correspond to a superficial velocity of 0.032 m/s. The superficial velocity of 0.042 m/s was attributed to a capacity of 0.072 mmol/g. The adsorption capacity was further enhanced to 0.076 mmol CO_2/g at a superficial velocity of 0.052 m/s.

It was observed that the feed superficial velocity plays a significant role in enhancing the adsorption capacity of the adsorbent.
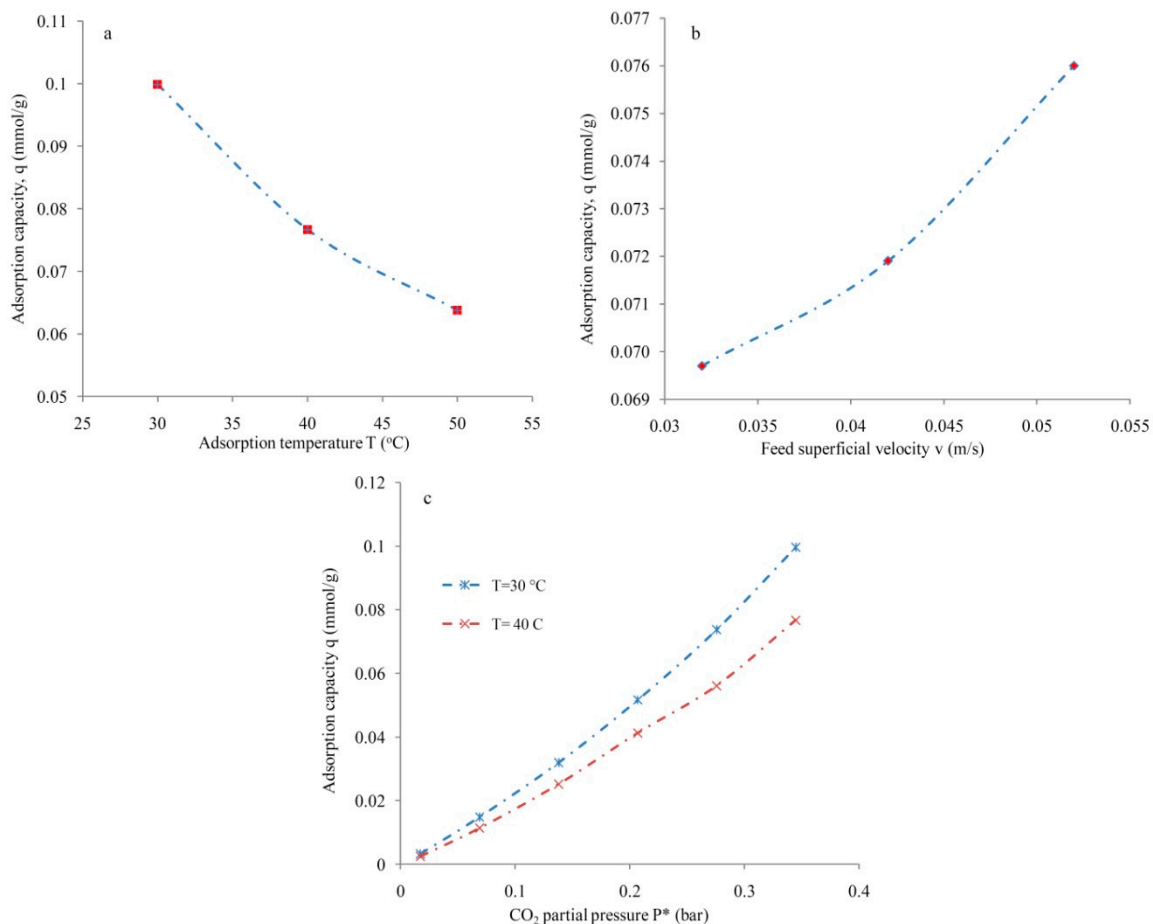

Figure 7. (**a**) Influence of bed temperature on bed capacity for SG ($v = 0.052$ m/s, $C_{in} = 5\%$); (**b**) influence of superficial velocity on adsorption capacity for SG (T = 40 °C); (**c**) adsorption isotherms for SG ($v = 0.052$ m/s).

The adsorption isotherms at the adsorption temperatures of 30 and 40 °C are shown in Figure 7c. The data were obtained at a fixed velocity of 0.052 m/s to analyze the influence of equilibrium partial pressure on capacity. It was observed that adsorption capacity was notably enhanced with the equilibrium partial pressure of the CO_2. Isotherms at an adsorption temperature of 30 °C exhibited a maximum capacity of 0.099 mmol/g with an equilibrium partial pressure of 0.345 bar. The adsorption capacity, equal to 0.003 mmol/g adsorbent up to the breakpoint, was determined. The isotherm at an adsorption temperature of 40 °C contributed to an adsorption capacity of 0.025 mmol/g at a partial pressure of 0.017 bar. The maximum adsorption capacity of 0.077 mmol/g was obtained at CO_2 partial pressure of 0.345 bar.

3.4. Repeatability and Accuracy Measurement

The repeatability measurement with a data point, N = 50, employing MS, was carried out (Figure 8). The experiments were conducted at a bed temperature and superficial velocity of 40 °C and 0.052 m/s, respectively. The inlet CO_2 composition in the feed was adjusted to 5%. The closeness of the data obtained for two different runs postulated the validity of the results obtained. In other words, these obtained data were reliable and valid. The coefficient of determination (R^2) was estimated to be equal to 0.996, which signifies the closeness of repeatability data obtained under Batch 1 and Batch 2. The mean error for repeatability measurements of C_{exit}/C_{in} was tabulated as equal to ±0.019.

The insignificant value of σ indicates that there is a good agreement between the obtained repeatability data. The repeatability is a measure of the consistency of the data. The uncertainty measurement of the sensors, i.e., temperature sensors, flow sensors (F1 and F2), and the IR meter, was carried out. The temperature sensor uncertainty in the mean was estimated to equal ±0.012 °C. The uncertainty in the mean for N_2 (F1) and CO_2 (F2) flow sensors corresponds to ±0.004 and ±0.002 L/min, respectively. The uncertainty in the measurement of CO_2 concentration (vol %) equals 0.174.
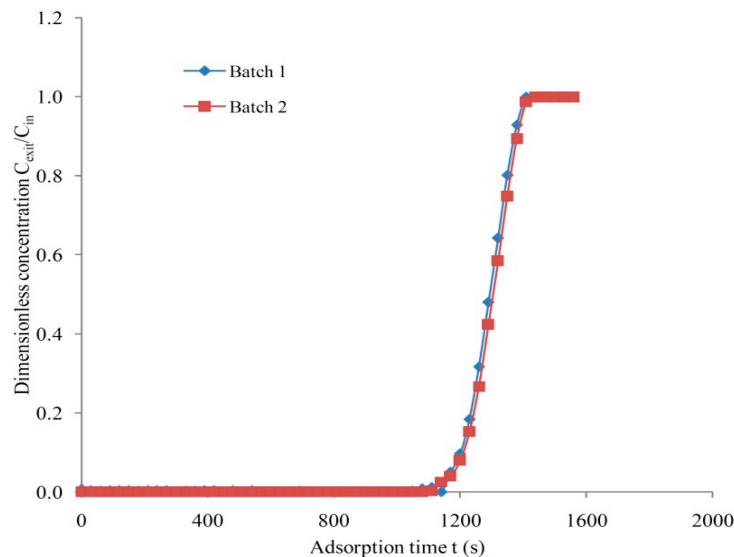
Figure 8. Repeatability measurement for MS (T = 40 °C, v = 0.042 m/s, C_{in} = 5%).

3.5. Mass Transfer Zone and Column Efficiency

In fixed-bed adsorption, the adsorbate concentrations in the fluid phase and solid phase vary with time as well as with the position in the bed. At first, the mass transfer largely takes place near the inlet of the bed, where fluid contacts fresh adsorbents. If the adsorbent contains no adsorbate at the start, the concentration in the fluid drops exponentially with distance, essentially to zero, before the end of the bed is approached. The section of the bed where CO_2 is essentially adsorbed or the region where most of the change in concentration occurs is recognized as the zone of mass transfer (L_{MTZ}) or the mass transfer zone. The major part of the adsorption at any time takes place in a relatively narrow adsorption zone known as the mass transfer zone (MTZ), and limits are frequently taken as C_{exit}/C_{in} = 0.95 to 0.05. A lean mass transfer zone means the proficient exploitation of the adsorbent, leading to the minimization of the energy regeneration cost [50,51]. The MTZ by and large moves from the input to the outlet all through the process, indicating that the adsorbent adjoining the input achieves the condition of saturation by CO_2; after that, the zone moves in the direction of the bed's end-side.

The efficiency based on column capacity or faction of total column capacity that is effectively used can be determined as

$$\eta = \frac{t_{ca}}{t_{st}} = \frac{\int_0^{t_{br}}\left(1 - \frac{C_{exit}}{C_{in}}\right)dt}{\int_0^{\infty}\left(1 - \frac{C_{exit}}{C_{in}}\right)dt} \tag{4}$$

The length of the adsorption column (L_{br}) used up to the breakpoint, or usable bed height, is determined using Equation (5):

$$L_{br} = \frac{t_{ca}}{t_{st}}L_{to} \tag{5}$$

where L_{to} denotes the total bed height. An unutilized bed height can be determined by Equation (6):

$$L_{ub} = \left(1 - \frac{t_{ca}}{t_{st}}\right)L_{to} \tag{6}$$

The lesser bed capacity is utilized as the width of the MTZ for concentration profile increases that correspond to an increased width of the breakthrough curve. Almost all of an adsorbent bed capacity is used before the breakthrough in the ideal case. The good adsorbent is characterized by the smaller width of the MTZ for the concentration profile, corresponding to the breakthrough profile. The steady pattern sorption of CO_2 was assumed for evaluating L_{MTZ}.

$$L_{MTZ} = \frac{2\,L(t_s - t_b)}{t_s + t_b} \tag{7}$$

The parameters of the CO_2 capture, i.e., effective column efficiency, L_{MTZ}, and usable bed height, were evaluated, as depicted in Table 3. The effective column efficiency alters considerably with temperature and feed rate. The maximal efficiency of 87.5% was determined for MS at 40 °C with v = 0.032 m/s. L_{MTZ} increases with increased temperature and superficial velocity, with minimal L_{MTZ} = 3.2 cm having a good usable height of 21 cm for MS. The reduced utilization factor of 0.432 was evaluated at the highest studied superficial velocity of 0.052 m/s at fixed operating conditions of temperature and initial CO_2 level. Lower column efficiency values were observed under various sets of operating conditions for SG, and the highest effective efficiency of 66.5% was determined. Additionally, the lowest L_{MTZ} = 9.65 cm was realized at 40 °C with v = 0.052 m/s, which is significantly higher relative to the lowest value of MS. The usable bed height of the total effective bed height of 24 cm is smaller for SG compared to the values determined for MS. Overall, under different operating conditions, smaller L_{MTZ} values signify the effective utilization of very good bed capacity at a breakthrough condition. This makes efficient use of an adsorbent and lowers the energy costs of regeneration.

Table 3. Characteristic parameters of CO_2 capture for MS and SG.

T (°C)	V (m/s)	C_{in}	MS			SG		
			η (%)	L_{MTZ} (cm)	L_{br} (cm)	η (%)	L_{MTZ} (cm)	L_{br} (cm)
30	0.052	5	86.1	3.58	20.66	57.8	12.05	13.87
40	0.052	5	84.8	3.94	20.35	66.5	9.65	15.96
50	0.052	5	83.9	4.18	20.14	44.7	18.34	10.73
40	0.032	5	87.5	3.20	21.00	65.6	9.94	15.74
40	0.042	5	86.2	3.55	20.69	56.1	13.49	13.46
40	0.052	5	84.6	4.02	20.30	64.5	10.37	15.48

4. Conclusions

The breakpoint time reduces significantly with increased bed temperature, and a prolonged breakthrough period contributes to an increased adsorption capacity. The maximum breakpoint periods of 1230 and 185 s were reported at a bed temperature of 30 °C for MS and SG, respectively, with a superficial velocity of 0.052 m/s. It was suggested that the breakpoint time would reduce with increased feed superficial velocity employing both the adsorbents. The prolonged breakpoint of 1515 s was noticed at a superficial feed velocity of 0.032 m/s, and it was reduced to 1185 s on raising the velocity to 0.042 m/s at a temperature of 40 °C for MS. It was noticed that the saturation adsorption capacity of CO_2 from the mixture of N_2 and CO_2 reduced appreciably with increased bed temperatures. The saturation adsorption capacity of MS adsorbent declined from 0.664 to 0.598 mmol/g, with an increase in bed temperature from 30 to 40 °C at a superficial velocity of 0.052 m/s.

It was observed that adsorption capacity increased remarkably with CO_2 partial pressure, commensurate with the isotherms at temperatures of 30 and 40 °C. At a partial pressure of 0.345 bar, the maximum capacity of 0.649 mmol/g was achieved at a temperature of 30 °C for MS. The smaller width of the MTZ of the MS adsorbent signifies the utilization of most of the bed capacity at the breakpoint compared to the relatively wider MTZ of SG. The lowest L_{MTZ} = 3.20 cm and the usable bed height of 21 cm, with good effective column efficiency of 87.5%, was determined for MS. It was

concluded that MS contributed to a higher adsorption capacity compared to SG, and it is suitable for the separation of CO_2 from a CO_2/N_2 mixture.

Conflicts of Interest: The authors declare that they have no conflict of interest.

References

1. Figueroa, J.D.; Fout, T.; Plasynski, S.; Mcllvried, H.; Srivastava, R.D. Advances in CO_2 capture technology—The US Department of Energy's Carbon Sequestration Program. *Int. J. Greenh. Gas Control* **2008**, *2*, 9–20. [CrossRef]
2. Zhou, L.; Lio, X.; Li, J.; Wang, N.; Wang, Z.; Zhou, Y. Synthesis of ordered mesoporous carbon molecular sieve and its adsorption capacity for H_2, N_2, O_2, CH_4, and CO_2. *Chem. Phys. Lett.* **2005**, *413*, 6–9. [CrossRef]
3. Chou, C.T.; Chen, C.Y. Carbon dioxide recovery by vacuum swing adsorption. *Sep. Purif. Technol.* **2004**, *39*, 51–65. [CrossRef]
4. Stewart, C.; Hessami, M.-A. A study of methods of carbon dioxide capture and sequestration-the sustainability of photosynthesis bioreactor approach. *Energy Convers. Manag.* **2005**, *46*, 403–420. [CrossRef]
5. Duffy, A.; Walker, G.M.; Allen, S.J. Investigation on the adsorption of acidic gases using activated dolomite. *Chem. Eng. J.* **2006**, *117*, 239–244. [CrossRef]
6. Thitakamol, B.; Veawab, A.; Aroonwilas, A. Environmental impacts of absorption-based CO_2 capture unit for post-combustion treatment of flue gas from goal fired-fired power plant. *Int. J. Greenh. Gas Control* **2007**, *1*, 318–342. [CrossRef]
7. Alabadi, A.; Razzaque, S.; Yang, Y.; Chen, S.; Tan, B. Highly porous activated carbon materials from carbonized biomass with high CO_2 capturing capacity. *Chem. Eng. J.* **2015**, *281*, 606–612. [CrossRef]
8. Gibbins, J.; Chalmers, H. Carbon capture and storage. *Energy Policy* **2008**, *36*, 4317–4322. [CrossRef]
9. Blomen, E.; Hendriksa, C.; Neele, F. Capture technologies: Improvement and promising developments. *Energy Procedia* **2009**, *1*, 1505–1512. [CrossRef]
10. Choi, W.J.; Seo, J.B.; Jang, S.Y.; Jung, J.H.; Oh, K.J. Removal characteristics of CO_2 using aqueous MEA/AMP solutions in the absorption and regeneration process. *J. Environ. Sci.* **2009**, *21*, 907–913. [CrossRef]
11. Brunetti, A.; Scura, F.; Barbieri, G.; Drioli, E. Membrane technologies for CO_2 separation. *J. Membr. Sci.* **2010**, *359*, 115–125. [CrossRef]
12. Xu, G.; Liang, F.; Yang, Y.; Hu, Y.; Zhang, K.; Liu, W. In improved CO_2 separation and purification system based on cryogenic separation and distillation theory. *Energies* **2014**, *7*, 3484–3502. [CrossRef]
13. Tiwari, D.; Goel, C.; Bhunia, H.; Bajpai, P.K. Novel nanostructured carbons derived from epoxy resin and their adsorption characteristics for CO_2 capture. *RSC Adv.* **2016**, *6*, 97728–97738. [CrossRef]
14. Yang, H.; Xu, Z.; Fan, M.; Gupta, R.; Slimane, R.B.; Bland, A.E.; Wright, I. Progress in carbon dioxide capture and separation: A review. *J. Environ. Sci.* **2008**, *20*, 14–27. [CrossRef]
15. Yamasaki, A. An overview of carbon dioxide mitigation options for global warming emphasizing carbon dioxide sequestration options. *J. Chem. Eng. Jpn.* **2003**, *36*, 361–375. [CrossRef]
16. MacDowell, N.; Florin, N.; Buchard, A.; Hallett, J.; Galindo, A.; Jackson, G.; Adjamin, C.; Williams, C.K.; Shah, N.; Fennel, P. An overview of carbon dioxide captures technologies. *Energy Environ. Sci.* **2010**, *3*, 1645–1669. [CrossRef]
17. Cohen, S.M.; Chalmers, H.L.; Webber, M.E.; King, C.W. Comparing post-combustion carbon dioxide capture operation at retrofitted coal-fired power in the Texas and Great Britain electric grids. *Environ. Res. Lett.* **2011**, *6*, 024001. [CrossRef]
18. Guo, B.; Chang, L.; Xie, K. Adsorption of carbon dioxide on activated carbon. *J. Nat. Gas Chem.* **2006**, *15*, 223–229. [CrossRef]

19. Gracia, S.; Gil, M.V.; Martin, C.F.; Pis, J.J.; Rubiera, F.; Pevida, C. Breakthrough adsorption study of a commercial activated carbon for pre-combustion carbon dioxide capture. *Chem. Eng. J.* **2011**, *171*, 549–556. [CrossRef]

20. Spin, M.J. Improving the gas solids contact efficiency in a fluidized bed of carbon dioxide adsorbent fine particles. *Phys. Chem. Chem. Phys.* **2011**, *13*, 4906–4909.

21. Ammendola, P.; Raganati, F.; Chrone, R.; Miccio, F. Fixed bed adsorption affected by thermodynamics and kinetics: Yellow tuff for CO_2 capture. *Powder Technol.* **2020**, *373*, 446–458. [CrossRef]

22. Sreenivasulu, B.; Gayatri, D.V.; Sreedhar, I.; Raghvan, K.V. A journey into the process and engineering aspects of carbon capture technologies. *Renew. Sustain. Energy Rev.* **2015**, *41*, 1324–1350. [CrossRef]

23. Li, J.; Ma, Y.; McCarthy, M.; Sculley, J.; Yu, J.; Jeong, H.; Balbuen, P.; Zhou, H. Carbon-dioxide-related gas adsorption and separation in metal-organic frameworks. *Coord. Chem. Rev.* **2011**, *255*, 1791–1823. [CrossRef]

24. Goetz, V.; Pupier, O.; Guillot, A. Carbon dioxide-methane mixture adsorption on activated carbon. *Adsorption* **2006**, *12*, 55–63. [CrossRef]

25. Al Mesfer, M.K. Synthesis and characterization of high-performance activated carbon from walnut shell biomass for CO_2 capture. *Environ. Sci. Pollut. Res.* **2020**, *27*, 15020–15028. [CrossRef]

26. Calvo-Munoz, E.M.; Garcia-Mateos, F.J.; Rosas, J.M.; Rodrigues-Mirasol, J.; Cordero, T. Biomass waste carbon materials as adsorbents for CO_2 capture under post-combustion conditions. *Front. Mater.* **2016**, *3*, 23. [CrossRef]

27. Raganati, F.; Alfe, M.; Gargiulo, V.; Chirone, R.; Ammendola, P. Kinetic study and breakthrough analysis of the hybrid physical/chemical CO_2 adsorption/desorption behavior of magnetite-based sorbent. *Chem. Eng. J.* **2019**, *372*, 526–535. [CrossRef]

28. Toprak, A.; Kopac, T. Carbon dioxide adsorption using high surface area activated carbons from local coals modified by KOH, NaOH and $ZnCl_2$ agents. *Int. J. Chem. React. Eng.* **2017**, *15*. [CrossRef]

29. Shen, C.; Yu, J.; Li, P.; Grande, C.A.; Rodrigues, A.E. Capture of CO_2 from flue gas by vacuum pressure swing adsorption using activated carbon beads. *Adsorption* **2011**, *17*, 179–188. [CrossRef]

30. Al Mesfer, M.K.; Danish, M.; Fahmy, M.Y.; Rashid, M.M. Post combustion CO_2 capture with activated carbons using fixed bed adsorption. *Heat Mass Transf.* **2018**, *54*, 2715–2724. [CrossRef]

31. Al Mesfer, M.K.; Danish, M. Breakthrough adsorption study of activated carbons for CO_2 separation from flue gas. *J. Environ. Chem. Eng.* **2018**, *6*, 4514–4524. [CrossRef]

32. Raganati, F.; Chirone, R.; Ammendola, P. CO_2 capture by temperature swing adsorption: Working capacity as affected by temperature and CO_2 partial pressure. *Ind. Eng. Chem. Res.* **2020**, *59*, 3593–3605. [CrossRef]

33. Raganati, F.; Ammendola, P.; Chirone, R. Effect of acoustic field on CO_2 desorption in fluidized bed of fine activated carbon. *Particulology* **2016**, *23*, 8–15. [CrossRef]

34. Shen, C.; Grande, C.A.; Li, P.; Yu, J.; Rodrigues, A.E. Adsorption equilibria and kinetics of CO_2 and N_2 on activated carbon beads. *Ind. Eng. Chem. Res.* **2010**, *47*, 4883–4890. [CrossRef]

35. Dantas, T.L.P.; Amorim, S.M.; Luna, F.M.T.; Silva, I.J., Jr.; Azevedo, D.C.S.; Rodrigues, A.E.; Morera, R.F.P.M. Adsorption of carbon dioxide onto activated carbon and nitrogen-enriched activated carbon-surface changes, equilibrium, and modeling of fixed bed adsorption. *Sep. Sci. Technol.* **2010**, *45*, 73–84. [CrossRef]

36. Reboldi, L.; Bolland, O. Evaluating pressure swing adsorption as a CO_2 separation technique in coal-fired power plants. *Int. J. Greenh. Gas Control* **2015**, *39*, 1–16. [CrossRef]

37. Sarkar, A.I.; Aroonwilas, A.; Veawab, A. Equilibrium and kinetic behavior of CO_2 adsorption onto zeolites, carbon molecular sieve and activated carbons. *Energy Procedia* **2017**, *114*, 2450–2459. [CrossRef]

38. Al-Janabi, N.; Vakili, R.; Kalumpasut, P.; Gorgojo, P.; Siperstein, F.R.; Fan, X. Velocity variation effect in fixed bed columns: A case study of CO_2 captures using porous solid adsorbents. *AIChE J.* **2018**, *64*, 2189–2197. [CrossRef]

39. Lu, C.; Bai, B.; Wu, B.; Su, F.; Hwang, J.F. Comparative study of CO_2 capture by carbon nanotubes, activated carbons, and zeolites. *Energy Fuels* **2008**, *22*, 3050–3056. [CrossRef]

40. Regufe, M.J.; Ferreira, A.F.P.; Lourero, J.M.; Shi, Y.; Rodrigues, A.; Ribeiro, A.M. New hybrid composite honeycomb monolith with 13X zeolite and activated carbon for CO_2 capture. *Adsorption* **2018**, *24*, 249–265. [CrossRef]

41. Xiang, S.; He, Y.; Zhang, Z.; Wu, H.; Zhou, W.; Krishna, R.; Chen, B. Microporous metal-organic framework with potential for carbon dioxide capture at ambient conditions. *Nat. Commun.* **2012**, *3*, 954. [CrossRef]

42. Yoro, K.O.; Singo, M.; Mulopo, J.L.; Daramola, M.O. Modeling and experimental study of the CO_2 adsorption behavior of polyaspartamide as an adsorbent during post-combustion CO_2 capture. *Energy Procedia* **2017**, *112*, 1643–1664. [CrossRef]

43. Monazam, E.R.; Spenik, J.; Shadle, L.J. Fluid bed adsorption of carbon dioxide on immobilized polyethylenimine (PEI): Kinetic analysis and breakthrough behavior. *Chem. Eng. J.* **2013**, *223*, 795–805. [CrossRef]

44. Harlick, P.J.E.; Tezel, F.H. An experimental adsorbent screening study for CO_2 removal from N_2. *Microporous Mesoporous Mater.* **2004**, *76*, 71–79. [CrossRef]

45. Cavenati, S.; Grande, C.A.; Rodrigues, A.E. Adsorption equilibrium of methane, carbon dioxide, and nitrogen on zeolite 13X at high pressures. *Chem. Eng. Data* **2004**, *49*, 1095–1101. [CrossRef]

46. Siriwardane, R.V.; Shen, M.S.; Fisher, E.P.; Poston, J.A. Adsorption of CO_2 on molecular sieves and activated carbon. *Energy Fuels* **2001**, *15*, 279–284. [CrossRef]

47. Kamiuto, K.; Abe, S. Effect of desorption temperature on CO_2 adsorption equilibria of the honeycomb zeolite beds. *Appl. Energy* **2002**, *72*, 555–564. [CrossRef]

48. Ertan, A. CO_2, N_2 and Ar Adsorption on Zeolites. Master's Thesis, Izmar Institute of Technology, Izmir, Turkey, 2004.

49. Li, Y.; Yi, H.; Tang, X.; Li, F.; Yuan, Q. Adsorption separation of CO_2/CH_4 gas mixture on the commercial zeolites at atmospheric pressure. *Chem. Eng. J.* **2013**, *229*, 50–56. [CrossRef]

50. Geankoplis, C.J. *Transport Processes and Unit Operations*, 3rd ed.; Printice-Hall International Inc.: Upper Saddle River, NJ, USA, 1993.

51. McCabe, W.L.; Smith, J.C.; Harriott, P. *Unit Operation of Chemical Engineering*, 5th ed.; McGraw-Hill Editions: Singapore, 1993.